Investigating the Osteoinductive Potential of a Decellularized Xenograft Bone Substitute

Daniel N. Bracey[1,*], Alexander H. Jinnah[1,*,†], Jeffrey S. Willey[2], Thorsten M. Seyler[3], Ian D. Hutchinson[4], Patrick W. Whitlock[5], Thomas L. Smith[1], Kerry A. Danelson[1], Cynthia L. Emory[1], Bethany A. Kerr [1,6,7,†]

[1] Wake Forest Baptist Medical Center, Orthopaedic Surgery, Winston Salem, NC, USA

[2] Wake Forest Baptist Medical Center, Radiation Oncology, Winston Salem, NC, USA

[3] Duke University, Orthopaedic Surgery, Durham, NC, USA

[4] Albany Medical Center, Orthopaedic Surgery, Albany, NY, USA

[5] Cincinnati Children's Hospital, Orthopaedic Surgery, Cincinnati, OH, USA

[6] Virginia Tech-Wake Forest University School for Bioengineering and Sciences, Winston Salem, NC, USA

[7] Wake Forest School of Medicine, Cancer Biology, Winston Salem, NC, USA

*Co-first authors

Short Title: Osteoinductivity in a Porcine Xenograft

[†]Corresponding Authors

Alexander H. Jinnah
Wake Forest Baptist Medical Center
Orthopaedic Surgery
1 Medical Center Blvd
Winston-Salem, NC, 27157, USA
Tel: 336-716-4025
Fax: 336-716-6110
E-mail: ajinnah@wakehealth.edu

Bethany A. Kerr
Wake Forest School of Medicine
Cancer Biology
1 Medical Center Blvd
Winston-Salem, NC, 27157, USA
Tel: 336-716-0320
Fax: 336-716-0255
Email: bkerr@wakehealth.edu

Keywords: bone scaffold, tissue engineering, osteoinductivity, bone microenvironment, angiogenesis

1. Abstract

Bone grafting is the second most common tissue transplantation procedure worldwide. The gold standard for bone grafting is the autograft; however, due to morbidity and limited supply, new alternatives, including allograft and tissue-engineered bone substitutes, are needed to satisfy long-term demand. One of the most desired properties of tissue-engineered bone substitutes is osteoinductivity, defined as the ability to stimulate primitive cells to differentiate into a bone forming lineage. In the current study, we treated porcine bone with a decellularization protocol to produce a bone scaffold. We examined whether the scaffold possessed osteoinductive potential and could be used to create a tissue-engineered bone microenvironment. To test if the bone scaffold was a viable host, pre-osteoblasts were seeded, incubated *in vitro*, and analyzed for markers of osteogenic differentiation. To assess these properties *in vivo*, scaffolds with and without pre-osteoblasts pre-seeded were subcutaneously implanted in mice for four weeks. The scaffolds underwent micro-computed tomography (microCT) scanning before implantation. After retrieval, the scaffolds were analyzed for osteogenic differentiation or re-scanned by microCT to assess new bone formation with the subsequent histological assessment. The osteoinductive potential was observed *in vitro* with similar osteogenic markers being expressed as observed in demineralized bone matrix and significantly greater expression of these markers than controls. By microCT, paired t-tests demonstrated significantly increased bone volume:total volume (BV/TV) and trabecular thickness (Tb.Th) after explantation in all groups. Pentachrome staining demonstrated osteogenesis within the scaffold, and angiogenesis in the scaffold was confirmed by CD31 staining for blood vessels. These results demonstrate that porcine bone maintains its osteoinductive properties after the application of a novel decellularization and oxidation protocol. Future work must be performed to definitively prove osteogenesis of human mesenchymal stem cells, biocompatibility in large animal models, and osteoinduction/osseointegration in a relevant clinical model *in vivo*. The ability to create a functional bone microenvironment using decellularized xenografts will impact regenerative medicine, orthopaedic reconstruction, and could be used in the research of multiple diseases.

2. Introduction

Regeneration and healing of critical bone defects resulting from high energy trauma, infection, necrosis, or tumor resection remain a major clinical challenge for orthopaedic surgeons [Calori et al., 2011; Kolambkar et al., 2011; Fassbender et al., 2014; Oryan et al., 2017]. The local biology in these defects is disrupted, rendering the self-regenerative healing cascade insufficient, and thus, conventional reparative techniques lead to nonunions, malunions, and osteomyelitis [Oryan et al., 2014; Oryan et al., 2017]. The gold standard treatment for a traumatic bone defect is the use of autologous bone graft; however, due to the associated morbidity and lack of adequate bone stock/donor sites, alternative grafts are commonly used. Alternative bone grafts include allografts and tissue-engineered bone substitutes [Calori et al., 2011; Roddy et al., 2018]. Allograft use risks disease transmission and has limited availability from young, healthy donors [De Long et al., 2007; Campana et al., 2014]. Consequently, there is increased interest in tissue-engineered bone substitutes [Wanschitz et al., 2007; Pina et al., 2017; Shahi et al., 2018; Iaquinta et al., 2019].

The ideal tissue-engineered bone substitute will be osteoconductive, osteoinductive, and osteogenic [Calori et al., 2011; Oryan et al., 2017]. Osteoconductivity is the ability for the bone graft to allow osseous growth on the surface or within its pores [Khan et al., 2005]. Osteogenic grafts retain living bone cells [Khan et al., 2005]. Osteoinductivity is the ability to stimulate progenitor cells to differentiate into a bone forming cell lineage [Albrektsson and Johansson, 2001; Khan et al., 2005]. Tissue-engineered bone replacements can be manufactured with customized structures for osteoconductivity and pre-seeded with osteogenic cells to establish osteogenicity prior to implantation [Zimmermann and Moghaddam, 2011]. Osteoinductivity, however, requires the construct to induce cell differentiation and therefore is more difficult to re-create [Albrektsson and Johansson, 2001; Fielding and Bose, 2013; Hsu et al., 2013; Oryan et al., 2017]. Xenograft derived tissue-engineered constructs are one potential way to utilize the natural osteoinductive properties of native bone. One ideal species for xenotransplantation is swine, due to physiologic compatibility with humans [Pierson et al., 2009; Wancket, 2015]. However; the presence of the alpha-gal epitope in porcine tissue can induce a severe inflammatory response in human hosts [Cooper et al., 2015; Vadori and Cozzi, 2015]. Our laboratory developed a decellularization protocol that sterilizes porcine soft tissues and removes the porcine DNA, including the alpha-gal epitope [Whitlock et al., 2007; Whitlock et al., 2012; Seyler et al., 2017].

60 We have applied this process to porcine cancellous bone and demonstrated that the construct
61 was successfully decellularized and maintained native structural properties, therefore preserving
62 the construct's osteoconductivity [Bracey et al., 2018]. This research project aimed to determine
63 whether the osteoinductive potential of the porcine-derived bone scaffold would be maintained
64 following application of a novel decellularization and oxidation technique in *in vitro* and *in vivo*
65 models.

66

67 ## 3. Materials and Methods

68 *Bone Scaffold Decellularization*

69 To generate the bone scaffolds, porcine tissues were processed by decellularization, and
70 oxidation using methods previously described [Whitlock et al., 2012; Seyler et al., 2017; Bracey et
71 al., 2018]. Briefly, the cancellous bone was harvested from the distal metaphysis of porcine
72 femurs and subjected to chemical decellularization and oxidation using combinations of deionized
73 water, trypsin, antimicrobials, peracetic acid (PAA), and triton-X. Scaffolds were lyophilized and
74 frozen at -80°C until further use. Scaffolds were cut to 1 cm diameter, and the thickness ranged
75 between 0.2 to 0.5 cm. The bone scaffolds were not decalcified at any point during this process.

76 *Cell Culture*

77 C2C12 and MC3T3-E1 cell lines were chosen for indirect quantification of the bone
78 scaffold's osteoinductive potential. C2C12 (CH3 genetic background, ATCC® CRL1772™, Rockville,
79 MD) is a mouse myoblast cell line that differentiates into osteoblasts in the presence of BMP-2
80 and is commonly used in osteoinduction studies [Katagiri et al., 1994; Han et al., 2003; Yang et al.,
81 2011; Shi et al., 2012; Ansari et al., 2013]. C2C12 cells were grown in DMEM media supplemented
82 with 10% FBS. MC3T3-E1 cells (ATCC® CRL1772™, Rockville, MD) were chosen as a second cell line
83 to confirm the bone scaffold's osteoinductive potential. These cells are an osteoblast precursor
84 derived from C57BL/6 mice and have previously been used to study osteoinductive potential as
85 well [Shuang et al., 2016; Araujo-Gomes et al., 2018]. MC3T3-E1 cells were grown in αMEM media
86 supplemented with 10% FBS and sodium pyruvate.

87 *Osteogenic Differentiation of C2C12 Cells*

88 Bone scaffolds or commercial grade cancellous demineralized bone matrix (DBM,
89 Musculoskeletal Transplant Foundation, Edison NJ) sheets (n=77 per group) were seeded with
90 $1x10^6$ C2C12 cells suspended in 100 µl cell culture media. DBM is commonly used in clinical
91 applications because of its reported osteoconductive and osteoinductive potential. Constructs
92 were moved into large Petri dishes, covered with DMEM + 10% FBS media, and returned to the
93 incubator. As a negative control, cells were also seeded onto gelfoam sponges (Cardinal Health)
94 which are assumed to have no or very limited biologic activity.

95 Constructs were incubated for 24 hours to allow cells to attach to the matrix. Sub-samples
96 from each group (n=11) were taken for analysis while the remaining were separated for continued
97 incubation in 2 different medias: 1) "Osteogenic Media (OM)" [Shui et al., 2013; Sondag et al.,
98 2013; Yu et al., 2013; Hupkes et al., 2014] consisting of DMEM with 10 mM β-Glycerophosphate
99 and 50 μg/mL ascorbic acid or 2) "BMP-2 Enriched Media" [Han et al., 2003; Feichtinger et al.,
100 2011; Yang et al., 2011; Ansari et al., 2013] consisting of the osteogenic media supplemented with
101 100 ng/mL BMP-2 (recombinant human BMP-2, 355-BM-050, R&D Systems). Media was replaced
102 every 3 days. The osteogenic media provided an environment supportive of osteogenic
103 differentiation while the BMP-2 enriched media served as a positive control to drive cells towards
104 osteoblastic lineage. Constructs (n=11) were harvested from each group at days 1, 3, 7, and 15 for
105 analysis of cell proliferation and osteogenic differentiation.

106 *Cell Viability and Proliferation on Scaffolds*

107 At each time point, constructs (n=2) from each group (n=6) were removed from their
108 respective dishes and individually rinsed with warm, sterile PBS. Constructs were then transferred
109 to chamber slides and incubated with the Live/Dead® Viability/Cytotoxicity Kit (Molecular Probes,
110 Eugene, OR) according to manufacturer's instructions. Specimens were immediately imaged on a
111 fluorescent confocal microscope (Zeiss Axiovert 100 M) to render cross-sectional 2D images as
112 well as projected 3D images. Live cells are labeled with the green calcein AM fluorophore, and
113 dead cells are labeled with the red ethidium homodimer-1 fluorophore.

114 DNA content was quantified from separate constructs (n=3) in each group to estimate cell
115 number and proliferation. Samples were flash frozen in liquid nitrogen, homogenized with a
116 sterilized tissue press, and lysed in 1 mL mammalian protein extraction reagent (M-PER®,
117 ThermoScientific, Waltham, MA). Samples were centrifuged 15 minutes at 13.2 kRPM and
118 supernatants were collected for analysis. DNA content was measured with Quant-iT™ PicoGreen®
119 dsDNA Assay Kit (Thermo Scientific) according to the manufacturer's instructions.

120 *Scanning Electron Microscopy and Scaffold Histology*

121 Cell attachment, morphology, and surface distribution were characterized by electron
122 microscopy. Specimens (n=2) were removed from dishes in each group at every time point, gently

123 washed with warmed sterile PBS and fixed in 2.5% glutaraldehyde for 3 hours and imaged on a
124 Hitachi S-2600 scanning electron microscope (SEM).

125 Specimens (n=2) from each group were removed from dishes, fixed in 10% formalin for
126 48 hours, decalcified with Immunocal® (Decal Chemical Cort, Tallman, NY) for 3-5 days, processed
127 and embedded in paraffin. Sections were mounted and stained with hematoxylin and eosin (H&E),
128 Masson's trichrome or 4',6-diamidino-2-phenylindole (DAPI) mounting media (ProLong® Gold
129 Antifade Mountant, Thermo Scientific). Representative light micrographs were captured with the
130 Olympus VS-110 Virtual Imaging System and fluorescent micrographs with a Zeiss Axioplan2
131 system.

132 *Alkaline Phosphatase Enzyme Assay and Immunohistochemistry*

133 The alkaline phosphatase (ALP) enzyme activity was measured from individual constructs
134 (n=3) using methods previously described [Liu et al., 2008; Stiehler et al., 2010; Thibault et al.,
135 2010; Arca et al., 2011; Marcos-Campos et al., 2012; Shi et al., 2013]. Each reaction was read in
136 triplicate by loading 150 µl from each tube into 96 well plates and measuring absorbance at 405
137 nm on a microplate reader (Spectra Max 340 PC). Cell-specific ALP activity was determined by
138 normalizing enzyme activity to the respective sample's DNA content determined by Pico Green
139 assay [Arca et al., 2011; Hashimoto et al., 2011; Kouroupis et al., 2013].

140 Immunohistochemistry (IHC) was performed with an anti-Placental ALP (Abcam ab16695,
141 Cambridge, United Kingdom) primary antibody that reacts with cell membrane-bound enzyme.
142 Secondary biotin-conjugated anti-rabbit antibody (BioGenex, Freemont, CA) was linked to HRP
143 (horseradish peroxidase) and developed with DAB (diaminobenzidine) substrate (Vector,
144 Burlingame, CA). Slides were counterstained with Mayer's Hematoxylin.

145 *Differentiation of MC3T3-E1 cells*

146 MC3T3-E1 cells ($1x10^6$) suspended in 250 µL of cell culture media were seeded and
147 incubated on scaffolds (n=18) for 1 hour before being submerged in 750 µL of α-MEM and
148 incubated at 37° C for 7 days. Control monolayers (n=9) of 1×10^6 cells plated on 10 µg/mL
149 collagen type I (Sigma) were also incubated at 37° C for 7 days in α-MEM. Cell culture media was
150 changed every 3 days.

151 *qPCR Analysis*

152 RNA was isolated from the scaffolds by grinding in liquid nitrogen followed by lysis in
153 Qiazol Reagent (RNeasy Microarray Tissue Mini Kit, QIAGEN, Hilden, Germany), and then RNA
154 purified following the manufacturer instructions for. RNA from monolayers was also isolated
155 following manufacturer instructions using the RNeasy Mini Kit. cDNA was produced through
156 reverse transcription using High Capacity cDNA Reverse Transcription Kit (Applied Biosystems)
157 and then analyzed for gene expression of different osteoblast markers using quantitative PCR.
158 Target gene expression was normalized to the housekeeping gene 18S ribosomal RNA (rRNA).
159 Primer sequences are available in Table 1. Relative gene expression was quantified by using the
160 $2^{-\Delta\Delta Ct}$ methodology originally described by Livak and Schmittgen [Livak and Schmittgen, 2001].

161 *Subcutaneous Implantation of Scaffolds*

162 To demonstrate cell viability and osteoinductivity *in vivo,* the scaffolds were either pre-
163 seeded (n=25) with MC3T3-E1 cells (1 x 10^6 suspended in 50 µL α-MEM) or not pre-seeded with
164 any cells (n=15). These scaffolds were then subcutaneously implanted in 7-week-old C57BL/6 mice
165 (Jackson Labs, Bar Harbor ME) for 4 weeks under a Wake Forest School of Medicine IACUC
166 Protocol #A16-197 (one scaffold per mouse).

167 *Micro-computed Tomography (microCT)*

168 A subset of scaffolds (n=12 pre-seeded, n=7 unseeded) underwent micro-computed-
169 tomography (microCT) scanning (TriFoil Imaging Triumph PET/CT, voxel size 1mm) before cell
170 seeding and implantation. Upon explantation, the constructs were placed in Buffer RLT (QIAGEN)
171 and vortexed to extract RNA or placed in 10% formalin to undergo microCT scanning to assess
172 new bone formation. For scaffolds that underwent microCT scanning, new bone formation was
173 assessed through the change in bone volume/total volume ratio (BV/TV) and trabecular thickness
174 (Tb.Th) using MicroView 3D Image Viewer and Analysis Tool (Parallax Innovations, Ilderton, ON,
175 Canada).

176 *Implanted Scaffold Histology and Immunohistochemistry*

177 Samples that underwent microCT scanning were fixed in 10% formalin overnight on a
178 shaker at 4°C and subsequently decalcified in 14% neutral, saturated EDTA for 7-14 days. Samples
179 were processed and embedded in paraffin. Sections were stained with Russel-Movat

180 Pentachrome (American MasterTech Scientific Inc; St. Lodi, CA). IHC was performed using primary
181 antibodies against osteopontin (OPN) (Abcam ab8448), ALP (R&D Systems FAB1448A) and CD31
182 (Abcam ab28364) to identify active bone remodeling, new bone formation, and angiogenesis.
183 Slides were scanned using a Hamamatsu NanoZoomer by the Virtual Microscopy Core.

184 *Statistical Analysis*

185 Multiple group comparisons were performed using one-way ANOVA, t-tests were
186 performed on independent means when comparing two groups, and paired t-tests were used
187 when comparing paired groups. Statistical significance was determined when α-error<0.05.
188 Graphs were prepared in GraphPad Prism 7.

189

190 ## 4. Results

191 *Scaffolds Support C2C12 Pre-Osteoblast Attachment, Survival, and Proliferation*

192 C2C12 pre-osteoblasts proliferated on scaffolds and deposited extracellular matrix (ECM)
193 components. Three-dimensional images of Live/Dead staining demonstrated circumferential cell
194 attachment evenly around the pores. In all constructs, the live (green) signal increased during
195 incubation with the strongest signal noted at day 15 (Figure 1). Dead (red) signal was strongest
196 on day 1, likely due to early contact inhibition after seeding constructs at a high cell density.
197 Additionally, all constructs displayed autofluorescence in the red channel as shown in the Blank
198 images (Figure 1). To assess proliferation on the constructs, DNA content was measured on the
199 three constructs over 15 days in the presence or absence of 100 ng/mL BMP-2 to induce
200 osteoblast differentiation. DNA content on DBM was greater than scaffolds at every time point,
201 indicating higher cell density (Figure 2). BMP-2 treatment had no consistent effect on cell
202 proliferation. Cells seeded on the scaffold proliferated, as demonstrated by increased DNA at each
203 time point with a 6.5-fold increase between days 1 and 15. The differences were significant
204 between day 1 and 15 ($p<0.01$) and day 3 and 15 ($p=0.01$). Similarly, DNA content on DBM
205 increased at each time point as well (Figure 2), while the gelfoam constructs demonstrated
206 increased DNA content at day 7 with a decrease at day 15. To confirm cell numbers and adhesion
207 to the constructs, C2C12 seeded DBM and decellularized bone scaffolds were examined. DAPI
208 and H&E staining (Figure 3) confirmed higher cell density on DBM relative to scaffolds indicating
209 that the increased cell proliferation is occurring in cells attached to the constructs. Finally,
210 scanning electron microscopy confirmed C2C12 adhesion to and spreading on the constructs.
211 Dense cell distribution was noted on DBM samples relative to scaffolds at day 7 and 15 (Figure 4).
212 ECM was deposited uniformly at later time points, and BMP-2 did not change cell morphology,
213 density, or distribution on matrices. Thus, the decellularized bone scaffolds were equally capable
214 of supporting pre-osteoblast adhesion and survival underscoring the osteogenic nature of the
215 scaffolds.

216 *Decellularized Bone Scaffolds Enhance Pre-Osteoblast Differentiation*

217 To examine the osteoinductive capacity of the decellularized bone scaffolds, C2C12 pre-
218 osteoblast differentiation on the constructs was compared. C2C12 cells were seeded onto either
219 DBM, bone scaffolds, or Gelfoam and grown in the presence or absence of BMP-2 for 15 days.

220 Molecular assays demonstrated that cells seeded on decellularized bone scaffolds had greater
221 ALP enzyme activity at day 7 (~40-fold) and day 15 (~25-fold) ($p<0.0001$) compared to cells seeded
222 on DBM or gelfoam constructs (Figure 5). BMP-2 increased ALP activity on all constructs, which
223 was only significant for scaffolds (days 3 ($p=0.005$), 7 ($p=0.02$), 15 ($p<0.0001$)) suggesting an
224 additive effect on this matrix. ALP IHC staining increased at day 15 in C2C12 cells seeded on bone
225 scaffolds and supported the above cell-specific enzyme activity findings (Figure 6). ALP staining
226 demonstrates darker staining on the scaffolds compared with DBM in the presence or absence of
227 BMP-2. Thus, the bone scaffolds support osteoblast differentiation of C2C12 cells.

228 To confirm the osteoinductive potential of the decellularized bone scaffolds, MC3T3-E1 pre-
229 osteoblast cells were grown on the scaffolds. Compared to cells grown in a monolayer on collagen
230 type I, MC3T3-E1 cells on the bone scaffolds expressed 2.5-fold higher *RANKL* and 2-fold higher
231 *BMP-2* (Figure 7). Taken together, these results indicate the bone construct possesses
232 osteoinductive potential *in vitro*.

233 *Implantation of Scaffolds in Syngeneic Mice Induces the Formation of a Bone Microenvironment*

234 Based on the osteogenic and osteoinductive capabilities of the decellularized bone scaffold,
235 we hypothesized that the seeded scaffold might be osteoconductive *in vivo*. MC3T3-E1 pre-
236 osteoblasts were seeded on bone scaffolds and implanted subcutaneously in syngeneic mice.
237 Unseeded scaffolds were implanted as controls. Upon removal, scaffolds were examined for
238 changes in osteoblast differentiation gene expression. *In vivo* expression of *ALP* (3.3-fold), *BMP-2*
239 (10.3-fold), and *BMP-7* (3.9-fold) increased within the pre-seeded scaffolds (Figure 8). *RANKL* gene
240 expression was equal between groups (data not shown). To assess changes in the bone structure
241 and measure possible bone formation, microCT analysis was performed on seeded (n=9) and un-
242 seeded (n=4) scaffolds (Figure 9). Increases in both bone volume fraction (BV/TV) and trabecular
243 thickness (Tb.Th) were seen in the pre-seeded scaffolds; however, only Tb.Th reached significance
244 ($p=0.03$). Paired t-tests showed significantly increased BV/TV (1.6-fold, $p=0.0013$) and Tb.Th (1.4-
245 fold, $p=0.0002$) after explantation when both groups are combined (n=13) indicating new bone
246 formation, regardless of cell seeding prior to implantation (Figure 9). After removal, scaffolds
247 were section and analyzed for osteogenesis and angiogenesis. Pentachrome staining of the
248 scaffolds displayed new bone formation within the pores of the scaffold in both groups (Figure
249 10A and 10C). To assess whether osteoclasts could be recruited to the scaffolds, staining for

250 tartrate-resistant acid phosphatase (TRAP) was performed. Small TRAP-positive cells were seen
251 within the pores and rare cells along the bone surface (Figure 10B and 10D). These cells likely
252 represent osteoclast progenitor cells, although no mature osteoclasts were seen within the four-
253 week time frame. Of note, pentachrome staining revealed apparent vascular-like structures
254 (Figure 11A and 11C) within the scaffold. IHC analysis demonstrated positive CD31 staining of
255 endothelial cells organized around a lumen and indicating angiogenesis within the decellularized
256 bone scaffold (Figure 11B and 11D). These results demonstrated that the scaffold maintains
257 osteoinductive potential following decellularization, due to its ability to recruit and stimulate cells
258 down a bone forming lineage *in vivo*. Further, implantation of the scaffold in a syngeneic host,
259 even without pre-osteoblast seeding, can generate a bone microenvironment.

260

261 ## 5. Discussion/Conclusion

262 Previously, our laboratory established a decellularization and oxidation technique using PAA
263 that removes 98% of DNA when applied to porcine bone [Bracey et al., 2018]. In this study, we
264 demonstrate that this protocol preserves the native bone's osteoinductive potential in a
265 decellularized scaffold. The decellularized bone scaffold supported pre-osteoblast adhesion,
266 survival, and proliferation comparable to DBM, a commercial product currently in clinical use with
267 proven osteoinductive potential. Further, the bone scaffold supported the development of a bone
268 microenvironment including osteogenesis, angiogenesis, and the recruitment of osteoclast
269 precursors. Thus, the decellularized bone scaffold is osteoconductive and osteoinductive.

270 Control of osteogenesis *in vitro* and *in vivo* is integral to regenerative medicine applications
271 in orthopaedic research. BMP-2 is one of the strongest stimulants of osteogenic differentiation in
272 the pre-osteoblast cell lines used in our experiments [Katagiri et al., 1994; Han et al., 2003;
273 Bormann et al., 2010; Qadir et al., 2015; Fu et al., 2017; Heo et al., 2018]. Concentrations as low
274 as 100 ng/mL and 50 ng/mL were sufficient to promote osteogenic differentiation with increased
275 ALP activity in MC3T3-E1 [Fu et al., 2017] and C2C12 [Han et al., 2003], respectively. However,
276 few reports studied osteogenic differentiation of cells seeded onto xenograft-derived bone
277 scaffolds [Arca et al., 2011; Hashimoto et al., 2011; Marcos-Campos et al., 2012; Kouroupis et al.,
278 2013; Lu et al., 2013]. Hashimoto et al. demonstrated porcine hydroxyapatite contains
279 osteoinductive properties and that these properties are maintained after processing [Hashimoto
280 et al., 2011]. Similarly, Smith et al. found the osteoinductive properties were maintained in
281 allografts following a decellularization and washing procedure [Smith et al., 2015]. However,
282 Bormann et al. used a similar decellularization and oxidation protocol to ours with the addition of
283 PAA on allografts and found the osteoinductive potential was not maintained [Bormann et al.,
284 2010]. In the present study, we applied a decellularization and oxidation technique using PAA that
285 removed 98% of the porcine DNA from the bone scaffolds [Bracey, 2017; Bracey et al., 2018].
286 Contrary to the findings by Borman et al. with human bone, our results demonstrate that the
287 xenograft does indeed maintain osteoinductive potential after processing. C2C12 and MC3T3-E1
288 cells attached to the scaffold matrix, proliferated, and underwent osteogenic differentiation
289 during the incubation period. The discrepancy between these studies outlines the variability
290 between decellularization techniques as well as donor species. Bormann et al. reported that the
291 donors ranged in both age (13-67 years) and gender, and ultimately concluded this could be a

292 source of variability between the human-derived samples. These discrepancies may affect
293 osteoinductive potential [Smith et al., 2017] and outline the importance of controlling
294 environmental factors that may influence the quality of the donor bone, which is possible with
295 the use of a xenograft.

296 Our *in vivo* microCT results demonstrated that there was equal osteogenesis identified in the
297 pre-seeded and unseeded scaffolds. This finding suggests that the scaffold alone recruits the
298 necessary cells for osteogenesis. Combining the microCT analysis and histologic assessment of the
299 porcine bone scaffold *in vivo* demonstrated spontaneous new bone formation and angiogenesis.
300 The identification of angiogenesis represents a critical finding due to the lack of vascularization
301 being one of the major limitations associated with the use of tissue-engineered constructs during
302 early bone regeneration [Muschler et al., 2004; Giannoni et al., 2010; Saran et al., 2014]. The
303 presence of angiogenesis signifies graft-host integration by the induction of inflammatory
304 cytokines as part of the normal healing process [Stegen et al., 2015]. It is reasonable to conclude
305 that the presence of angiogenesis allowed for new bone formation due to the known importance
306 angiogenesis has in bone repair and regeneration [Saran et al., 2014; Stegen et al., 2015].
307 Accordingly, Hirata et al. found that a BMP-2 soaked absorbable collagen sponge implanted in
308 humans led to new bone formation lined by endothelial cells [Hirata et al., 2017]. Furthermore,
309 Bhumiratana et al. implanted a clinically approved decellularized bovine trabecular bone seeded
310 with adipose-derived stem cells into Yucatan minipig skull defects and concluded that
311 angiogenesis and new bone formation occurred in parallel [Bhumiratana et al., 2016]. Thus, our
312 decellularized bone scaffold represents a potential tissue-engineered bone microenvironment
313 capable of both angiogenesis and osteogenesis. The angiogenesis demonstrated in these
314 experiments may be due to the complex inflammatory response between the decellularized
315 scaffold and M1 and M2 macrophages, and IL-4. This has been previously demonstrated within
316 decellularized bone scaffold implants [Zheng et al., 2018], but is beyond the scope of this
317 investigation.

318 There are limitations to our study. First, clinical translation of *in vitro* and animal experiments
319 is limited. However, we believe these experiments are a necessary step to determine the
320 properties of this bone scaffold after undergoing the decellularization and oxidation procedure.
321 Second, our *in vivo* experiments involve an ectopic subcutaneous implantation model, rather than
322 an orthotopic bone void filling model. However, the purpose of these experiments was solely to

323 determine the osteoinductive potential of this scaffold in an *in vitro* and *in vivo* environment.
324 Finally, a major limitation is using murine rather than human cell lines for these experiments,
325 which limits immediate clinical translation. These cell lines, however, have been validated for the
326 study of biomaterial osteoinductive potential previously [Qadir et al., 2015; Kanayama et al.,
327 2017]. Despite these limitations, the decellularized porcine bone scaffold can be used in future
328 experiments to assess its clinical and therapeutic utility.

329 Overall, our data demonstrate that a decellularization and oxidation technique applied to
330 porcine metaphyseal bone preserves the osteoinductive potential of the bone. Previous literature
331 identified that these properties are the most difficult to artificially create in tissue-engineered
332 scaffolds and to maintain when processing bone scaffolds, therefore outlining the potential
333 clinical impact of this construct. Future studies involving this xenograft will focus on placing the
334 construct within a bone defect, identifying osseointegration, and comparing it to current standard
335 treatments. These experiments will look at the effect of supplementing the scaffold with human
336 mesenchymal stem cells, as a step towards clinical translation. Furthermore, an *in vivo* analysis of
337 inflammatory markers to confirm that the bone scaffold has no increased reactivity when
338 compared to currently used clinical implants for large bone defects should be performed. Further
339 research will determine whether this decellularized bone scaffold capable of osteoinductivity and
340 osteogenesis is fully osteoconductive and able to function as a substitute bone
341 microenvironment.

342 ## 8. Statements

343 ### 8.1. Acknowledgments

344 We would like to thank Ms. Eileen Elsner, Ms. Jiaozhong Cia, and Dr. Lihong Shi for their help with
345 tissue processing and animal handling throughout these experiments. We thank Brandi Bickford from
346 the Virtual Microscopy Core for her assistance in slide scanning.

347 ### 8.2. Statement of Ethics

348 All animal experiments conform to internationally accepted standards, and the study protocol was
349 approved by the Wake Forest School of Medicine IACUC.

350 ### 8.3. Disclosure Statement

351 Dr. Patrick Whitlock has a patent which covers the intellectual property associated with the
352 decellularization protocol used in this work. Patent #: US20070248638A1.

353 ### 8.4. Funding Sources

354 We thank the Orthopaedic Research and Education Foundation (OREF) and AO Trauma North America
355 for their contribution to the funding of this project through a Resident Clinician Scientist Research
356 Grant to D.N.B.. We would also like to thank the Musculoskeletal Transplant Foundation (MTF) for their
357 donation of human DBM samples at no cost. The animal experiments were supported by a CTSI Ignition
358 Fund under the NIH/NCATS UL1 TR001420 grant to B.A.K.. None of the funding sources have been
359 given the manuscript to review. The funding bodies have been given periodic updates on our work.

360 ### 8.5. Author Contributions

361 Dr. Jinnah and Dr. Bracey had substantial contributions to the conception, acquisition, analysis, and
362 interpretation of the work. Together they drafted the original manuscript and assisted with ongoing
363 revisions. Dr. Willey contributed to analysis and interpretation of data and critical revisions to the
364 manuscript. Dr. Seyler substantially contributed to the conception and design of the work and critical
365 revisions to the manuscript. Dr. Hutchinson substantially contributed to the conception and design of
366 the work and critical revisions to the manuscript. Dr. Whitlock substantially contributed to the
367 conception and design of the work, interpretation of data, and critical revisions to the manuscript. Dr.
368 Smith substantially contributed to the conception and design of the work, analysis of data, and critical
369 revisions to the manuscript. Dr. Danelson substantially contributed to the analysis of the work and
370 critical revisions to the manuscript. Dr. Emory substantially contributed to the interpretation of the
371 work and critical revisions to the manuscript. Dr. Kerr substantially contributed to the conception and
372 design of the work, analysis, interpretation of data, and critical revisions to the manuscript. All authors

373 approved the final version of the manuscript for publication and agreed to be accountable for all
374 aspects of the work.

9. References

Albrektsson, T., C. Johansson (2001) Osteoinduction, osteoconduction and osseointegration. Eur Spine J *10 Suppl 2*: S96-101.

Ansari, S., A. Moshaverinia, S.H. Pi, A. Han, A.I. Abdelhamid, H.H. Zadeh (2013) Functionalization of scaffolds with chimeric anti-BMP-2 monoclonal antibodies for osseous regeneration. Biomaterials *34(38)*: 10191-10198.

Araujo-Gomes, N., F. Romero-Gavilan, I. Garcia-Arnaez, C. Martinez-Ramos, A.M. Sanchez-Perez, M. Azkargorta, F. Elortza, J.J.M. de Llano, M. Gurruchaga, I. Goni, J. Suay (2018) Osseointegration mechanisms: a proteomic approach. Journal of biological inorganic chemistry : JBIC : a publication of the Society of Biological Inorganic Chemistry.

Arca, T., J. Proffitt, P. Genever (2011) Generating 3D tissue constructs with mesenchymal stem cells and a cancellous bone graft for orthopaedic applications. Biomed Mater *6(2)*: 025006.

Bhumiratana, S., J.C. Bernhard, D.M. Alfi, K. Yeager, R.E. Eton, J. Bova, F. Shah, J.M. Gimble, M.J. Lopez, S.B. Eisig, G. Vunjak-Novakovic (2016) Tissue-engineered autologous grafts for facial bone reconstruction. Science translational medicine *8(343)*: 343ra383.

Bormann, N., A. Pruss, G. Schmidmaier, B. Wildemann (2010) In vitro testing of the osteoinductive potential of different bony allograft preparations. Archives of orthopaedic and trauma surgery *130(1)*: 143-149.

Bracey, D.N. (2017) A Decellularized Porcine Xenograft-Derived Bone Scaffold for Clinical Use as a Bone Graft Substitute: A Critical Evaluation of Processing and Structure: Orthopaedic Surgery, Wake Forest University Graduate School of Arts & Sciences.

Bracey, D.N., T.M. Seyler, A.H. Jinnah, M.O. Lively, J.S. Willey, T.L. Smith, M.E. Van Dyke, P.W. Whitlock (2018) A Decellularized Porcine Xenograft-Derived Bone Scaffold for Clinical Use as a Bone Graft Substitute: A Critical Evaluation of Processing and Structure. Journal of functional biomaterials *9(3)*.

Calori, G.M., E. Mazza, M. Colombo, C. Ripamonti (2011) The use of bone-graft substitutes in large bone defects: any specific needs? Injury *42 Suppl 2*: S56-63.

Campana, V., G. Milano, E. Pagano, M. Barba, C. Cicione, G. Salonna, W. Lattanzi, G. Logroscino (2014) Bone substitutes in orthopaedic surgery: from basic science to clinical practice. J Mater Sci Mater Med *25(10)*: 2445-2461.

Cooper, D.K.C., B. Ekser, A.J. Tector (2015) Immunobiological barriers to xenotransplantation. International journal of surgery *23(Pt B)*: 211-216.

De Long, W.G., Jr., T.A. Einhorn, K. Koval, M. McKee, W. Smith, R. Sanders, T. Watson (2007) Bone grafts and bone graft substitutes in orthopaedic trauma surgery. A critical analysis. The Journal of bone and joint surgery American volume *89(3)*: 649-658.

Fassbender, M., S. Minkwitz, M. Thiele, B. Wildemann (2014) Efficacy of two different demineralised bone matrix grafts to promote bone healing in a critical-size-defect: a radiological, histological and histomorphometric study in rat femurs. International orthopaedics *38(9)*: 1963-1969.

Feichtinger, G.A., T.J. Morton, A. Zimmermann, D. Dopler, A. Banerjee, H. Redl, M. van Griensven (2011) Enhanced reporter gene assay for the detection of osteogenic differentiation. Tissue engineering Part C, Methods *17(4)*: 401-410.

Fielding, G., S. Bose (2013) SiO2 and ZnO dopants in three-dimensionally printed tricalcium phosphate bone tissue engineering scaffolds enhance osteogenesis and angiogenesis in vivo. Acta biomaterialia *9(11)*: 9137-9148.

Franceschi, R.T., B.S. Iyer, Y. Cui (1994) Effects of ascorbic acid on collagen matrix formation and osteoblast differentiation in murine MC3T3-E1 cells. Journal of bone and mineral research : the official journal of the American Society for Bone and Mineral Research *9(6)*: 843-854.

Fu, C., X. Yang, S. Tan, L. Song (2017) Enhancing Cell Proliferation and Osteogenic Differentiation of MC3T3-E1 Pre-osteoblasts by BMP-2 Delivery in Graphene Oxide-Incorporated PLGA/HA Biodegradable Microcarriers. Scientific reports *7(1)*: 12549.

Giannoni, P., S. Scaglione, A. Daga, C. Ilengo, M. Cilli, R. Quarto (2010) Short-time survival and engraftment of bone marrow stromal cells in an ectopic model of bone regeneration. Tissue engineering Part A *16(2)*: 489-499.

Han, B., B. Tang, M.E. Nimni (2003) Quantitative and sensitive in vitro assay for osteoinductive activity of demineralized bone matrix. J Orthop Res *21(4)*: 648-654.

Hashimoto, Y., S. Funamoto, T. Kimura, K. Nam, T. Fujisato, A. Kishida (2011) The effect of decellularized bone/bone marrow produced by high-hydrostatic pressurization on the osteogenic differentiation of mesenchymal stem cells. Biomaterials *32(29)*: 7060-7067.

Heo, S.Y., S.C. Ko, S.Y. Nam, J. Oh, Y.M. Kim, J.I. Kim, N. Kim, M. Yi, W.K. Jung (2018) Fish bone peptide promotes osteogenic differentiation of MC3T3-E1 pre-osteoblasts through upregulation of MAPKs and Smad pathways activated BMP-2 receptor. Cell biochemistry and function *36(3)*: 137-146.

Hirata, A., T. Ueno, P.K. Moy (2017) Newly Formed Bone Induced by Recombinant Human Bone Morphogenetic Protein-2: A Histological Observation. Implant dentistry *26(2)*: 173-177.

Hsu, E.L., J.H. Ghodasra, A. Ashtekar, M.S. Nickoli, S.S. Lee, S.I. Stupp, W.K. Hsu (2013) A comparative evaluation of factors influencing osteoinductivity among scaffolds designed for bone regeneration. Tissue engineering Part A *19(15-16)*: 1764-1772.

Hupkes, M., A.M. Sotoca, J.M. Hendriks, E.J. van Zoelen, K.J. Dechering (2014) MicroRNA miR-378 promotes BMP2-induced osteogenic differentiation of mesenchymal progenitor cells. BMC Mol Biol *15(1)*: 1.

Iaquinta, M.R., E. Mazzoni, M. Manfrini, A. D'Agostino, L. Trevisiol, R. Nocini, L. Trombelli, G. Barbanti-Brodano, F. Martini, M. Tognon (2019) Innovative Biomaterials for Bone Regrowth. International journal of molecular sciences *20(3)*.

Kanayama, S., T. Kaito, K. Kitaguchi, H. Ishiguro, K. Hashimoto, R. Chijimatsu, S. Otsuru, S. Takenaka, T. Makino, Y. Sakai, A. Myoui, H. Yoshikawa (2017) ONO-1301 Enhances in vitro Osteoblast Differentiation and in vivo Bone Formation Induced by Bone Morphogenetic Protein. Spine.

Katagiri, T., A. Yamaguchi, M. Komaki, E. Abe, N. Takahashi, T. Ikeda, V. Rosen, J.M. Wozney, A. Fujisawa-Sehara, T. Suda (1994) Bone morphogenetic protein-2 converts the differentiation pathway of C2C12 myoblasts into the osteoblast lineage. J Cell Biol *127(6 Pt 1)*: 1755-1766.

Khan, S.N., F.P. Cammisa, Jr., H.S. Sandhu, A.D. Diwan, F.P. Girardi, J.M. Lane (2005) The biology of bone grafting. The Journal of the American Academy of Orthopaedic Surgeons *13(1)*: 77-86.

Kolambkar, Y.M., K.M. Dupont, J.D. Boerckel, N. Huebsch, D.J. Mooney, D.W. Hutmacher, R.E. Guldberg (2011) An alginate-based hybrid system for growth factor delivery in the functional repair of large bone defects. Biomaterials *32(1)*: 65-74.

Kouroupis, D., T.G. Baboolal, E. Jones, P.V. Giannoudis (2013) Native multipotential stromal cell colonization and graft expander potential of a bovine natural bone scaffold. Journal of orthopaedic research : official publication of the Orthopaedic Research Society.

Liu, G., J. Sun, Y. Li, H. Zhou, L. Cui, W. Liu, Y. Cao (2008) Evaluation of partially demineralized osteoporotic cancellous bone matrix combined with human bone marrow stromal cells for tissue engineering: an in vitro and in vivo study. Calcified tissue international *83(3)*: 176-185.

Livak, K.J., T.D. Schmittgen (2001) Analysis of relative gene expression data using real-time quantitative PCR and the 2(-Delta Delta C(T)) Method. Methods (San Diego, Calif) *25(4)*: 402-408.

Lu, X., J. Wang, B. Li, Z. Zhang, L. Zhao (2013) Gene expression profile study on osteoinductive effect of natural hydroxyapatite. J Biomed Mater Res A.

Marcos-Campos, I., D. Marolt, P. Petridis, S. Bhumiratana, D. Schmidt, G. Vunjak-Novakovic (2012) Bone scaffold architecture modulates the development of mineralized bone matrix by human embryonic stem cells. Biomaterials *33(33)*: 8329-8342.

Muschler, G.F., C. Nakamoto, L.G. Griffith (2004) Engineering principles of clinical cell-based tissue engineering. The Journal of bone and joint surgery American volume *86-A(7)*: 1541-1558.

Oryan, A., S. Alidadi, A. Moshiri, N. Maffulli (2014) Bone regenerative medicine: classic options, novel strategies, and future directions. Journal of orthopaedic surgery and research *9(1)*: 18.

Oryan, A., A. Kamali, A. Moshiri, M. Baghaban Eslaminejad (2017) Role of Mesenchymal Stem Cells in Bone Regenerative Medicine: What Is the Evidence? Cells, tissues, organs *204(2)*: 59-83.

Pierson, R.N., 3rd, A. Dorling, D. Ayares, M.A. Rees, J.D. Seebach, J.A. Fishman, B.J. Hering, D.K. Cooper (2009) Current status of xenotransplantation and prospects for clinical application. Xenotransplantation *16(5)*: 263-280.

Pina, S., R.F. Canadas, G. Jimenez, M. Peran, J.A. Marchal, R.L. Reis, J.M. Oliveira (2017) Biofunctional Ionic-Doped Calcium Phosphates: Silk Fibroin Composites for Bone Tissue Engineering Scaffolding. Cells, tissues, organs *204(3-4)*: 150-163.

Qadir, A.S., S. Um, H. Lee, K. Baek, B.M. Seo, G. Lee, G.S. Kim, K.M. Woo, H.M. Ryoo, J.H. Baek (2015) miR-124 negatively regulates osteogenic differentiation and in vivo bone formation of mesenchymal stem cells. J Cell Biochem *116(5)*: 730-742.

Roddy, E., M.R. DeBaun, A. Daoud-Gray, Y.P. Yang, M.J. Gardner (2018) Treatment of critical-sized bone defects: clinical and tissue engineering perspectives. European journal of orthopaedic surgery & traumatology : orthopedie traumatologie *28(3)*: 351-362.

Saran, U., S. Gemini Piperni, S. Chatterjee (2014) Role of angiogenesis in bone repair. Archives of biochemistry and biophysics *561*: 109-117.

Seyler, T.M., D.N. Bracey, J.F. Plate, M.O. Lively, S. Mannava, T.L. Smith, J.M. Saul, G.G. Poehling, M.E. Van Dyke, P.W. Whitlock (2017) The Development of a Xenograft-Derived Scaffold for Tendon and Ligament Reconstruction Using a Decellularization and Oxidation Protocol. Arthroscopy : the journal of arthroscopic & related surgery : official publication of the Arthroscopy Association of North America and the International Arthroscopy Association *33(2)*: 374-386.

Shahi, M., M. Nadari, M. Sahmani, E. Seyedjafari, N. Ahmadbeigi, A. Peymani (2018) Osteoconduction of Unrestricted Somatic Stem Cells on an Electrospun Polylactic-Co-Glycolic Acid Scaffold Coated with Nanohydroxyapatite. Cells, tissues, organs *205(1)*: 9-19.

Shi, K., J. Lu, Y. Zhao, L. Wang, J. Li, B. Qi, H. Li, C. Ma (2013) MicroRNA-214 suppresses osteogenic differentiation of C2C12 myoblast cells by targeting Osterix. Bone *55(2)*: 487-494.

Shi, Q., Y. Li, J. Sun, H. Zhang, L. Chen, B. Chen, H. Yang, Z. Wang (2012) The osteogenesis of bacterial cellulose scaffold loaded with bone morphogenetic protein-2. Biomaterials *33(28)*: 6644-6649.

Shuang, Y., L. Yizhen, Y. Zhang, M. Fujioka-Kobayashi, A. Sculean, R.J. Miron (2016) In vitro characterization of an osteoinductive biphasic calcium phosphate in combination with recombinant BMP2. BMC oral health *17(1)*: 35.

Shui, W., W. Zhang, L. Yin, G. Nan, Z. Liao, H. Zhang, N. Wang, N. Wu, X. Chen, S. Wen, Y. He, F. Deng, J. Zhang, H.H. Luu, L.L. Shi, Z. Hu, R.C. Haydon, J. Mok, T.C. He (2013) Characterization of scaffold carriers for BMP9-transduced osteoblastic progenitor cells in bone regeneration. J Biomed Mater Res A.

Smith, C.A., T.N. Board, P. Rooney, M.J. Eagle, S.M. Richardson, J.A. Hoyland (2017) Human decellularized bone scaffolds from aged donors show improved osteoinductive capacity compared to young donor bone. PloS one *12(5)*: e0177416.

Smith, C.A., S.M. Richardson, M.J. Eagle, P. Rooney, T. Board, J.A. Hoyland (2015) The use of a novel bone allograft wash process to generate a biocompatible, mechanically stable and osteoinductive biological scaffold for use in bone tissue engineering. Journal of tissue engineering and regenerative medicine *9(5)*: 595-604.

Sondag, G.R., S. Salihoglu, S.L. Lababidi, D.C. Crowder, F.M. Moussa, S.M. Abdelmagid, F.F. Safadi (2013) Osteoactivin Induces Transdifferentiation of C2C12 Myoblasts into Osteoblasts. J Cell Physiol.

Stegen, S., N. van Gastel, G. Carmeliet (2015) Bringing new life to damaged bone: the importance of angiogenesis in bone repair and regeneration. Bone *70*: 19-27.

Stiehler, M., F.P. Seib, J. Rauh, A. Goedecke, C. Werner, M. Bornhauser, K.P. Gunther, P. Bernstein (2010) Cancellous bone allograft seeded with human mesenchymal stromal cells: a potential good manufacturing practice-grade tool for the regeneration of bone defects. Cytotherapy *12(5)*: 658-668.

Thibault, R.A., L. Scott Baggett, A.G. Mikos, F.K. Kasper (2010) Osteogenic differentiation of mesenchymal stem cells on pregenerated extracellular matrix scaffolds in the absence of osteogenic cell culture supplements. Tissue engineering Part A *16(2)*: 431-440.

Torii, Y., K. Hitomi, N. Tsukagoshi (1994) L-ascorbic acid 2-phosphate promotes osteoblastic differentiation of MC3T3-E1 mediated by accumulation of type I collagen. Journal of nutritional science and vitaminology *40(3)*: 229-238.

Vadori, M., E. Cozzi (2015) The immunological barriers to xenotransplantation. Tissue antigens *86(4)*: 239-253.

Wancket, L.M. (2015) Animal Models for Evaluation of Bone Implants and Devices: Comparative Bone Structure and Common Model Uses. Vet Pathol *52(5)*: 842-850.

Wanschitz, F., E. Stein, W. Sutter, D. Kneidinger, K. Smolik, F. Watzinger, D. Turhani (2007) Expression patterns of Ets2 protein correlate with bone-specific proteins in cell-seeded three-dimensional bone constructs. Cells, tissues, organs *186(4)*: 213-220.

Whitlock, P.W., T.M. Seyler, G.D. Parks, D.A. Ornelles, T.L. Smith, M.E. Van Dyke, G.G. Poehling (2012) A novel process for optimizing musculoskeletal allograft tissue to improve safety, ultrastructural properties, and cell infiltration. The Journal of bone and joint surgery American volume *94(16)*: 1458-1467.

Whitlock, P.W., T.L. Smith, G.G. Poehling, J.S. Shilt, M. Van Dyke (2007) A naturally derived, cytocompatible, and architecturally optimized scaffold for tendon and ligament regeneration. Biomaterials *28(29)*: 4321-4329.

Yang, Q., J. Jian, S.B. Abramson, X. Huang (2011) Inhibitory effects of iron on bone morphogenetic protein 2-induced osteoblastogenesis. J Bone Miner Res *26(6)*: 1188-1196.

Yu, S., Q. Geng, J. Ma, F. Sun, Y. Yu, Q. Pan, A. Hong (2013) Heparin-binding EGF-like growth factor and miR-1192 exert opposite effect on Runx2-induced osteogenic differentiation. Cell Death Dis *4*: e868.

Zimmermann, G., A. Moghaddam (2011) Allograft bone matrix versus synthetic bone graft substitutes. Injury *42 Suppl 2*: S16-21.

10. Figure Legends

Table 1. qPCR primer sequences

Primer	Sequence
Alkaline Phosphatase (forward)	GGCAGCGTCAGATGTTAATTG
Alkaline Phosphatase (reverse)	ACTGCGCTCCTTAGGGCT
Bone Morphogenetic Protein-7 (forward)	CTTGGAAAGATCAAACCGGA
Bone Morphogenetic Protein-7 (reverse)	GGACAGCCACTTCCTCACTG
Bone Morphogenetic Protein-2 (forward)	GAAGTTCCTCCACGGCTTCT
Bone Morphogenetic Protein-2 (reverse)	AGATCTGTACCGCAGGCACT
Receptor activator of nuclear factor κ B ligand (forward)	AGGCTGGGCCAAGATCTCTA
Receptor activator of nuclear factor κ B ligand (reverse)	GTCTGTAGGTACGCTTCCCG
18s (forward)	GCGGTTCTATTTTGTTGGTTT
18s (reverse)	CTCCGACTTTCGTTCTTGATT

Figure 1. C2C12 cells are viable on the decellularized bone scaffold.

Demineralized Bone Matrix (DBM), scaffold, and gelfoam matrices were seeded with 1 million C2C12 pre-osteoblast cells, incubated for 1, 3, 7, or 15 days. On day 1, matrices were switched into osteogenic media (OM) enriched with 100 ng/mL BMP-2. Representative micrographs show green fluorophore (calcein AM) staining of live cells and red fluorophore (ethidium) staining of dead cells. Constructs had notable autofluorescence with ethidium staining as shown in the "blank" images. Cross-sectional images were captured at 10X magnification and overlayed to create the shown 3D projections. Cell density increased with time on all 3 matrices, consistent with DNA quantification results.

Figure 2. C2C12 cells proliferate slowly on the decellularized bone constructs.

DBM (red bars), bone scaffold (blue bars), or gelfoam (GF; white bars) constructs were harvested at days 1, 3, 7, and 15, and treated with control media, osteogenic media (OM), or OM with 100 ng/mL BMP-2. DNA content was measured with the PicoGreen® assay and represented as mean DNA content ± SEM. * represents $p<0.05$, ** represents <0.01, and *** represents $p<0.001$.

(a) scaffold vs DBM; **(b)** scaffold vs GF; **(c)** DBM vs GF

(d) scaffold OM vs BMP; **(e)** DBM OM vs BMP; **(f)** GF OM vs BMP;

(g) DBM day 1 vs 3; **(h)** scaffold day 1 vs 3; **(i)** GF day 1 vs 3;

(j) DBM day 3 vs 7; **(k)** scaffold day 3 vs 7; **(l)** GF day 3 vs 7

(m) DBM day 7 vs 15; **(n)** scaffold day 7 vs 15; **(o)** GF day 7 vs 15

(p) scaffold day 3 vs 15; **(q)** DBM day 3 vs 15; **(r)** GF day 3 vs 15

Figure 3. C2C12 cell density is increased on DBM compared with scaffolds.

C2C12 cells were seeded on DBM (left panels) or decellularized bone scaffold (right panels). Seeded scaffolds were sectioned and stained for DAPI (top panels) or H&E (bottom panels). Representative images are shown taken at 10X (top panels) or 5X (bottom panels).

Figure 4. C2C12 attachment and spreading is equivalent on bone constructs and DBM

C2C12 seeded DBM and bone scaffolds were analyzed by scanning electron microscopy at days 1, 7, or 15 and compared to unseeded scaffolds. Comparison with 100 ng/mL BMP-2 treated scaffolds are shown. Representative images at 30X (scale bar represents 1 mm), 100X (scale bar represents 500 µm), and 1000X (scale bar represents 50 µm) are shown.

Figure 5. Scaffolds induce ALP activity in C2C12 cells.

C2C12 seeded constructs: DBM (red bars), bone scaffolds (blue bars), or Gelfoam (white bars), were incubated in osteogenic media (A) or in the presence of 100 ng/mL BMP-2 (B) and analyzed for enzymatic ALP activity represented as mean p-nitrophenyl phosphate (pNPP) content ± SEM. * represents $p<0.05$, ** represents <0.01, and *** represents $p<0.001$.

(a) scaffold vs DBM; **(b)** scaffold vs GF; **(c)** DBM vs GF

(d) scaffold OM vs BMP; **(e)** DBM OM vs BMP; **(f)** GF OM vs BMP;

(g) DBM day 1 vs 3; **(h)** scaffold day 1 vs 3; **(i)** GF day 1 vs 3;

(j) DBM day 3 vs 7; **(k)** scaffold day 3 vs 7; **(l)** GF day 3 vs 7

(m) DBM day 7 vs 15; **(n)** scaffold day 7 vs 15; **(o)** GF day 7 vs 15

(p) scaffold day 3 vs 15; **(q)** DBM day 3 vs 15; **(r)** GF day 3 vs 15

Figure 6. **ALP expression increases over time in both DBM and scaffolds.**

DBM (left panels) or decellularized bone (right panels) scaffolds were sectioned unseeded, after 1-day culture of C2C12 cells or after 15 days in OM or OM with 100 ng/mL BMP-2. Sections were stained for ALP expression by immunohistochemistry and representative images are shown at 4X, 10X, 20X, or 40X.

Figure 7. Scaffolds induce MC3T3-E1 osteogenic differentiation.

MC3T3-E1 cells were seeded on 10 µg/mL collagen I (black bars) or decellularized bone scaffolds (gray bars) for one week. Gene expression of *BMP-2* (A) and *RANKL* (B) were measured and represented as mean fold change normalized to *18S* ± SEM.

Figure 8. Implantation of scaffolds *in vivo* induces osteogenic gene expression.

Bone scaffolds were seeded with MC3T3-E1 pre-osteoblast cells (gray bars) or left unseeded (black bars) and implanted subcutaneously in syngeneic mice. After 4 weeks scaffolds were removed, processed, and analyzed for gene expression of *ALP* (A), *BMP–2* (B), and *BMP-7* (C) represented as mean fold change normalized to *18S* ± SEM. * represents $p<0.05$.

Figure 9. New bone formation occurs in implanted bone constructs.

Bone scaffold structure was analyzed by microCT (pre-implantation) and then implanted subcutaneously in mice either unseeded (open squares) or pre-seeded with MC3T3-E1 pre-osteoblast cells (closed circles). Implants were removed after 4 weeks and scanned again by microCT (post-explantation). Bone volume ratio (BV/TV, A) and trabecular thickness (Tb.Th, B) were calculated and the change between individual scaffolds is shown.

Figure 10. Implantation of bone scaffolds induces a functional bone microenvironment.

MC3T3-E1 seeded and unseeded scaffolds were removed from mice after 4 weeks and processed for histology. Sections were stained with Movat's pentachrome (A and C) to visualize the extracellular matrix deposition in the scaffolds. Arrows show the area of new bone formation in scaffold which stains green in representative photos captured at 10X. (B and D) Sections were also stained for osteoclasts using TRAP enzyme activity. Arrows point to purple staining demonstrating small TRAP-positive cells in the pores and along the bone surface in representative photos taken at 20X.

Figure 11. Angiogenesis occurs in the implanted bone scaffolds

MC3T3-E1 seeded and unseeded scaffolds were removed from mice after 4 weeks and processed for immunohistochemistry (IHC) for the endothelial marker CD31. In the representative micrographs at 20X, Movat's pentachrome (A and C) demonstrate small vessels indicated with arrows, and corresponding IHC for CD31 confirms that these are endothelial cells (B and D).

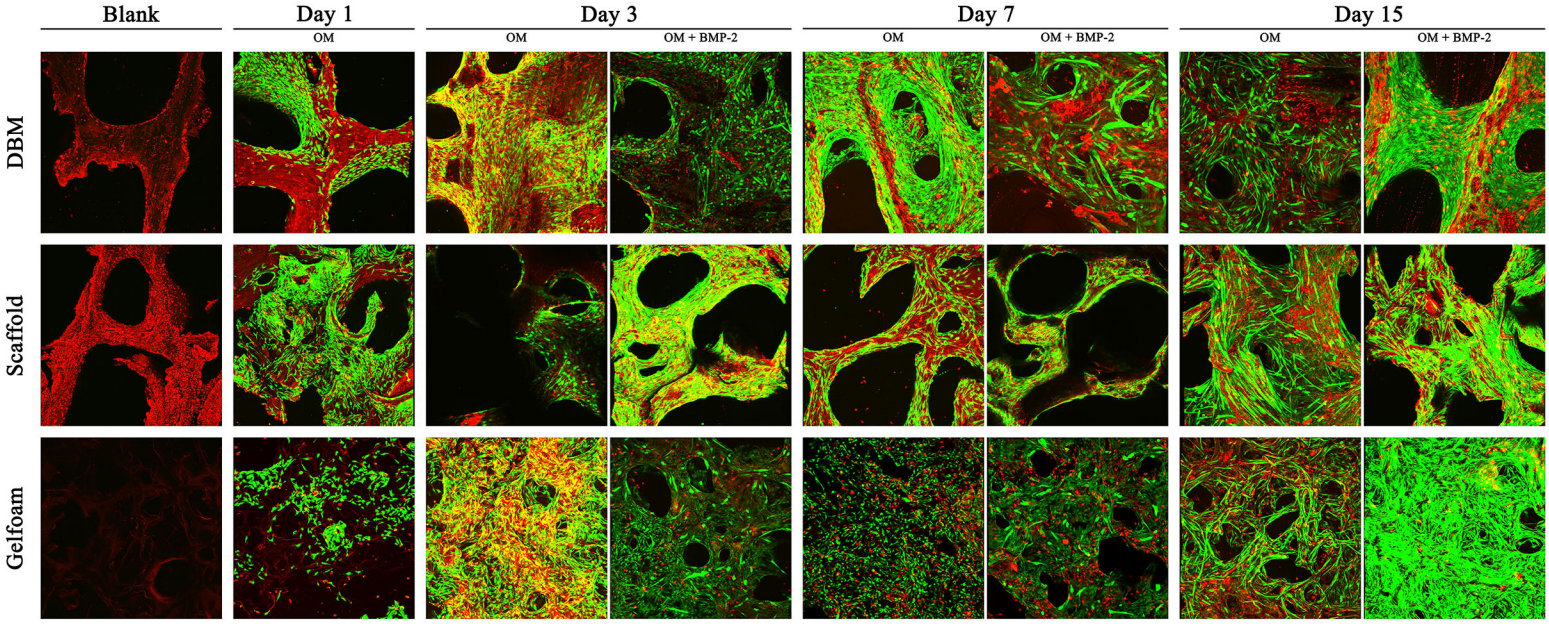
Blank
Day 1
Day 3
Day 7
Day 15
OM
OM
OM + BMP-2
OM
OM + BMP-2
OM
OM + BMP-2
DBM
Scaffold
Gelfoam

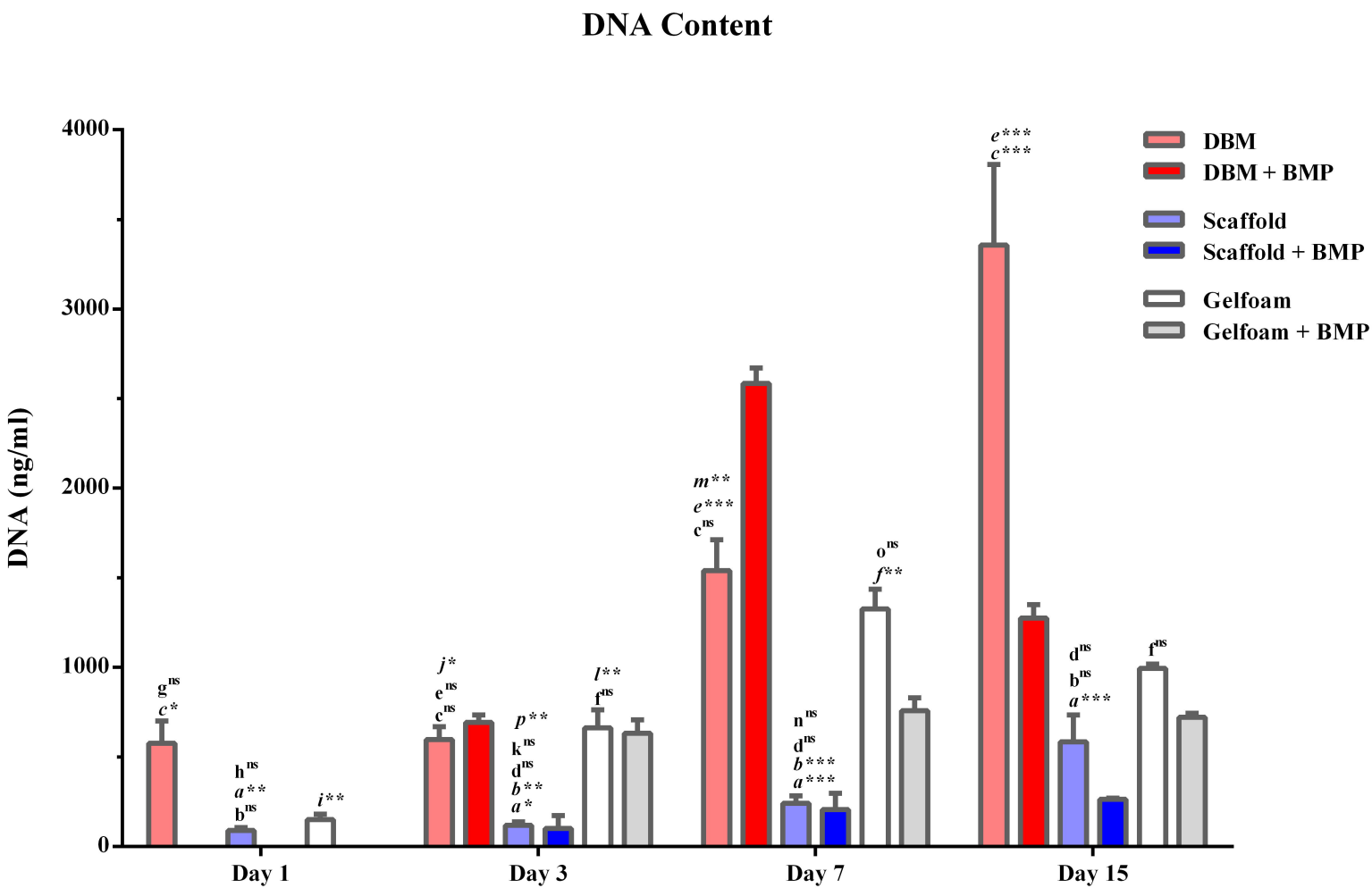
DNA Content
DNA (ng/ml)
4000
3000
2000
1000
0
Day 1
Day 3
Day 7
Day 15
DBM
DBM + BMP
Scaffold
Scaffold + BMP
Gelfoam
Gelfoam + BMP
g ns
c *
h ns
a **
b ns
i **
j *
e ns
c ns
p **
k ns
d ns
b **
a *
l **
f ns
m **
e ***
c ns
n ns
d ns
b ***
a ***
o ns
j **
e ***
c ***
d ns
b ns
a ***
f ns

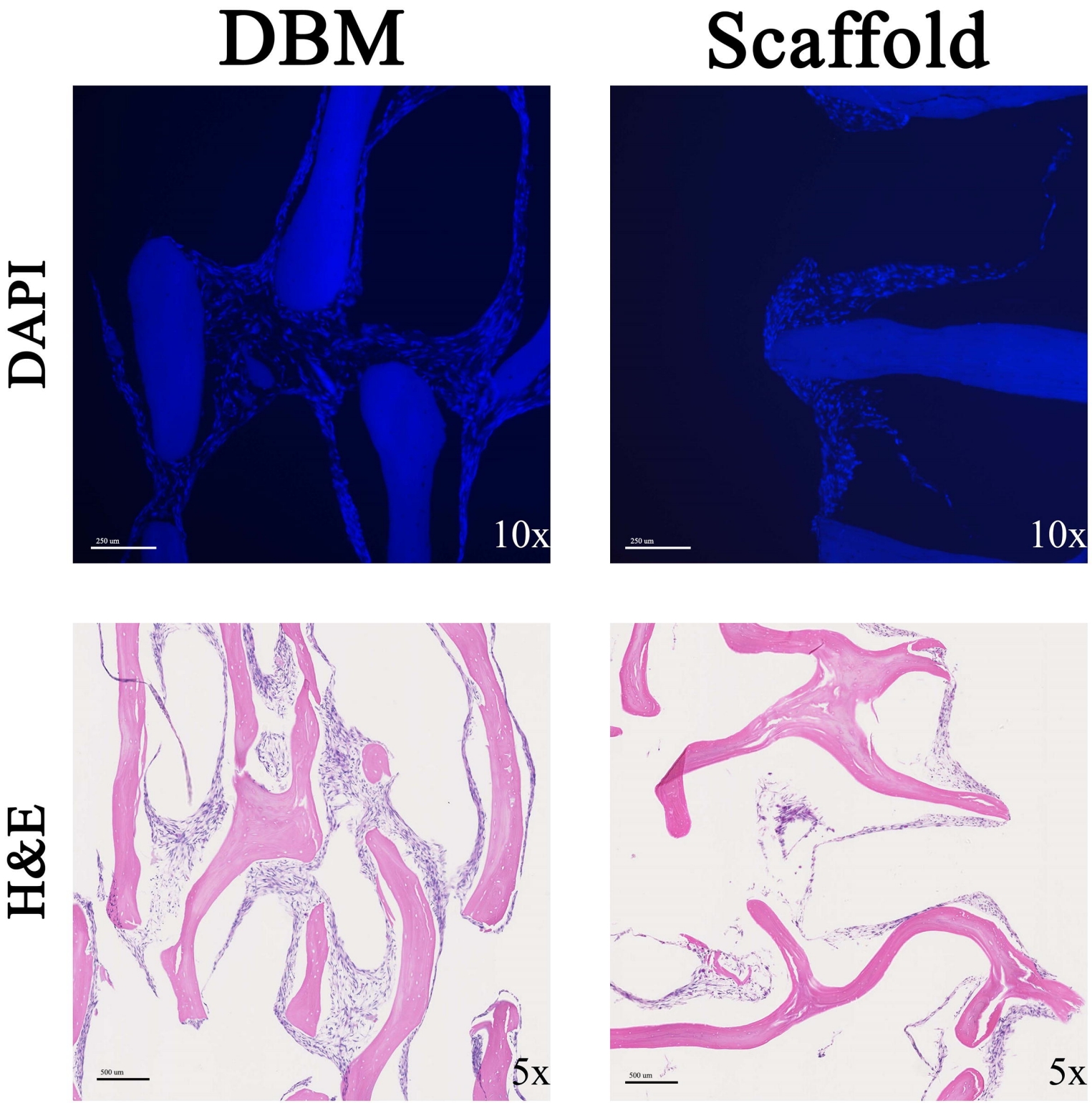
DBM
Scaffold
DAPI
H&E
250 um
10x
250 um
10x
500 um
5x
500 um
5x

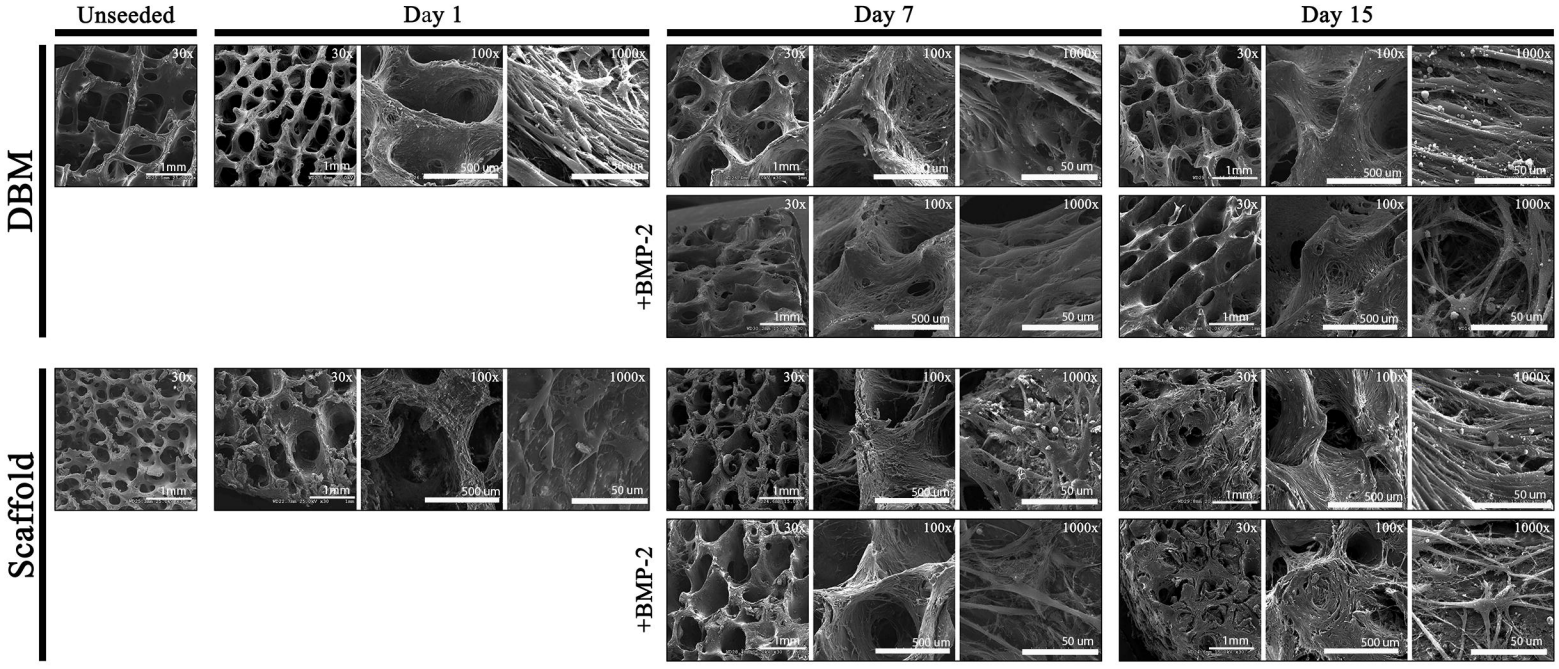
Unseeded
Day 1
Day 7
Day 15
DBM
+BMP-2
Scaffold
+BMP-2
30x
100x
1000x
1mm
500 um
50 um

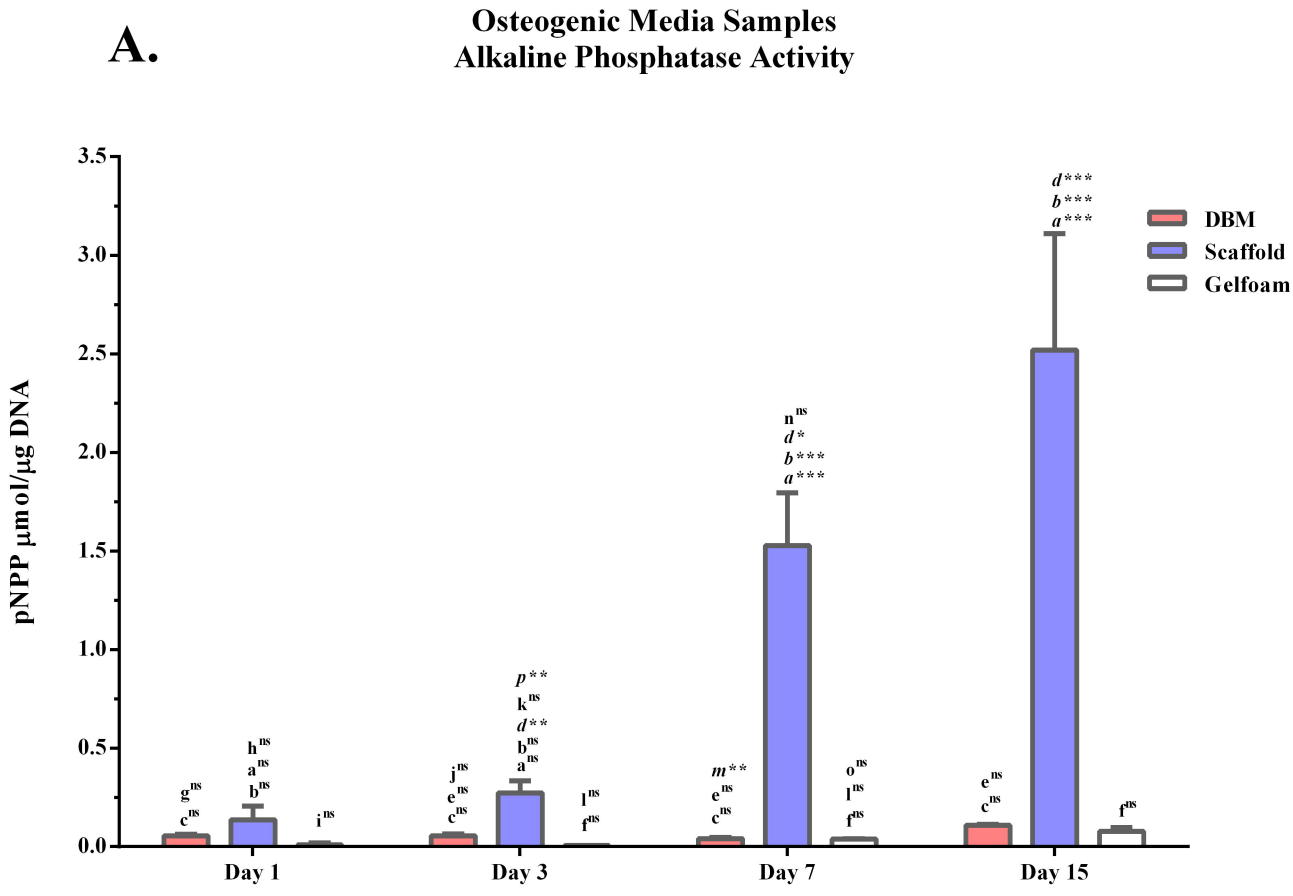
A.
Osteogenic Media Samples
Alkaline Phosphatase Activity
pNPP µmol/µg DNA
3.5
3.0
2.5
2.0
1.5
1.0
0.5
0.0
DBM
Scaffold
Gelfoam
Day 1
Day 3
Day 7
Day 15

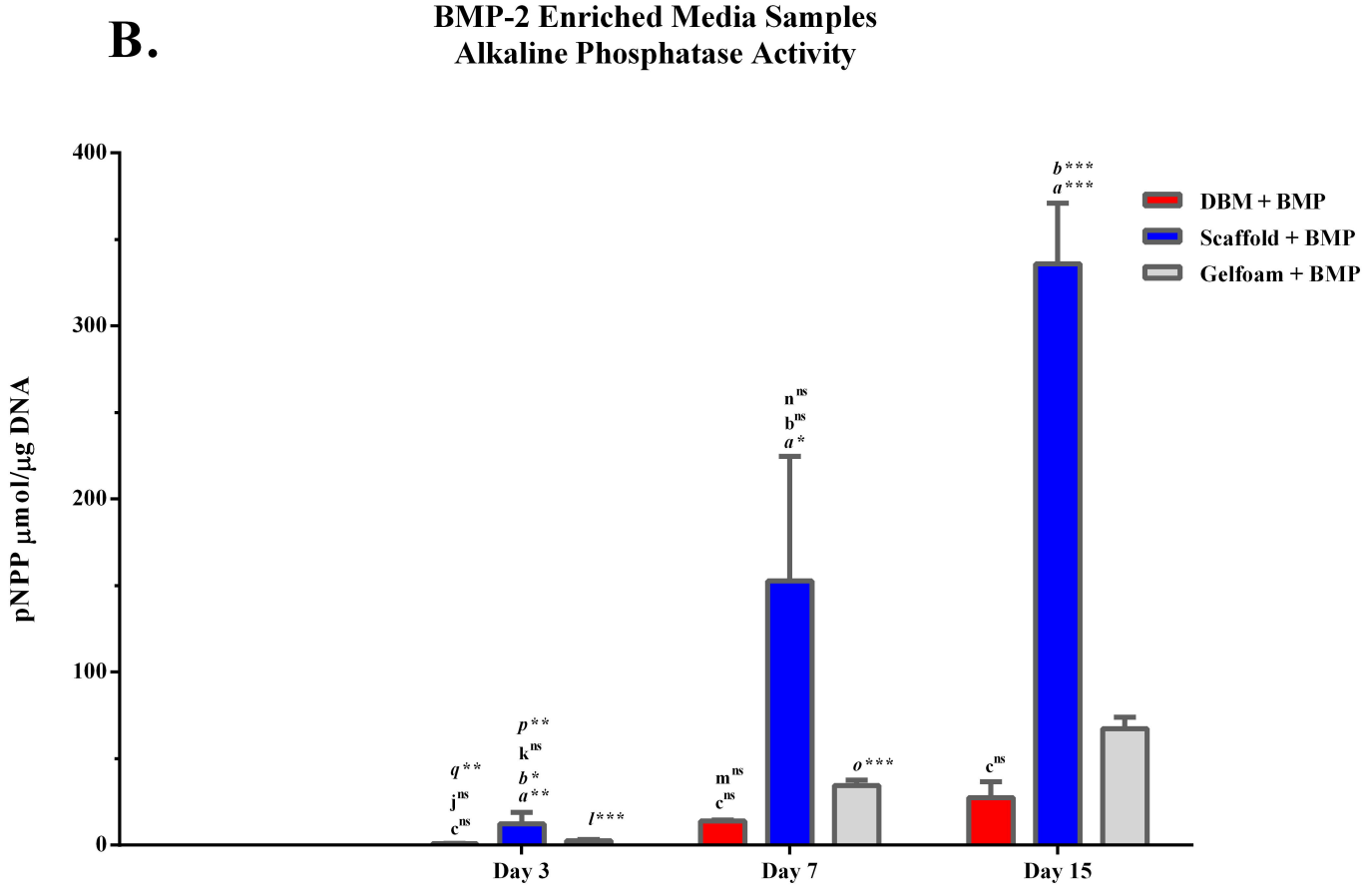
B.
BMP-2 Enriched Media Samples
Alkaline Phosphatase Activity
pNPP µmol/µg DNA
400
300
200
100
0
DBM + BMP
Scaffold + BMP
Gelfoam + BMP
Day 3
Day 7
Day 15

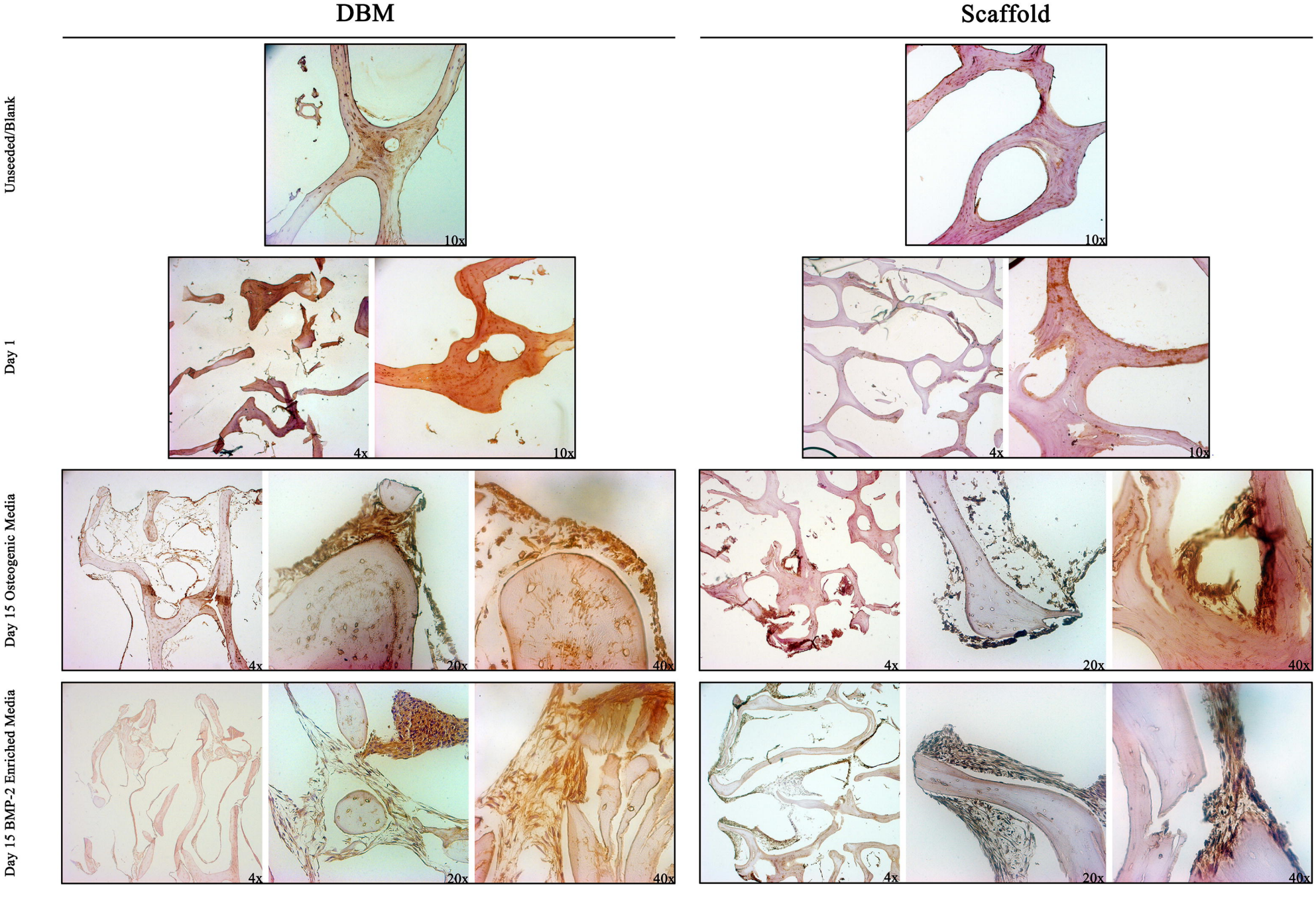
DBM
Scaffold
Unseeded/Blank
Day 1
Day 15 Osteogenic Media
Day 15 BMP-2 Enriched Media
10x
4x
10x
4x
10x
4x
20x
40x
4x
20x
40x
4x
20x
40x
4x
20x
40x

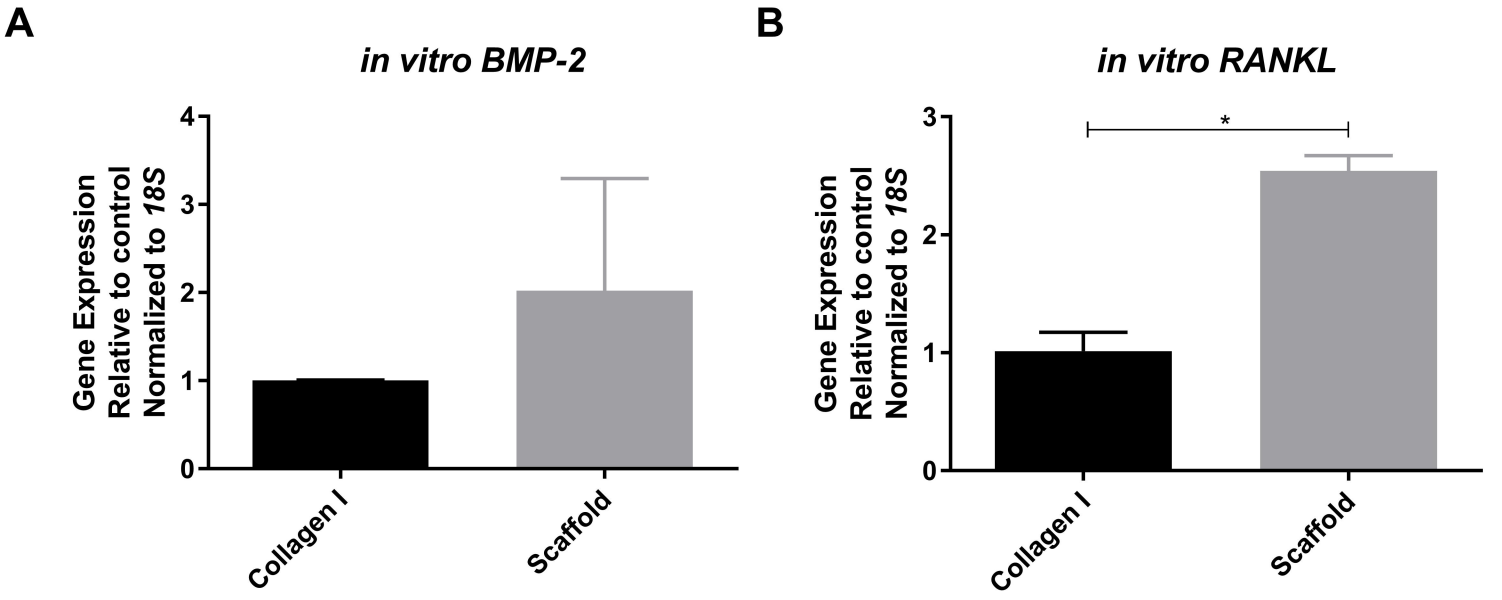
A
in vitro BMP-2
Gene Expression
Relative to control
Normalized to 18S
0
1
2
3
4
Collagen I
Scaffold
B
in vitro RANKL
Gene Expression
Relative to control
Normalized to 18S
0
1
2
3
*
Collagen I
Scaffold

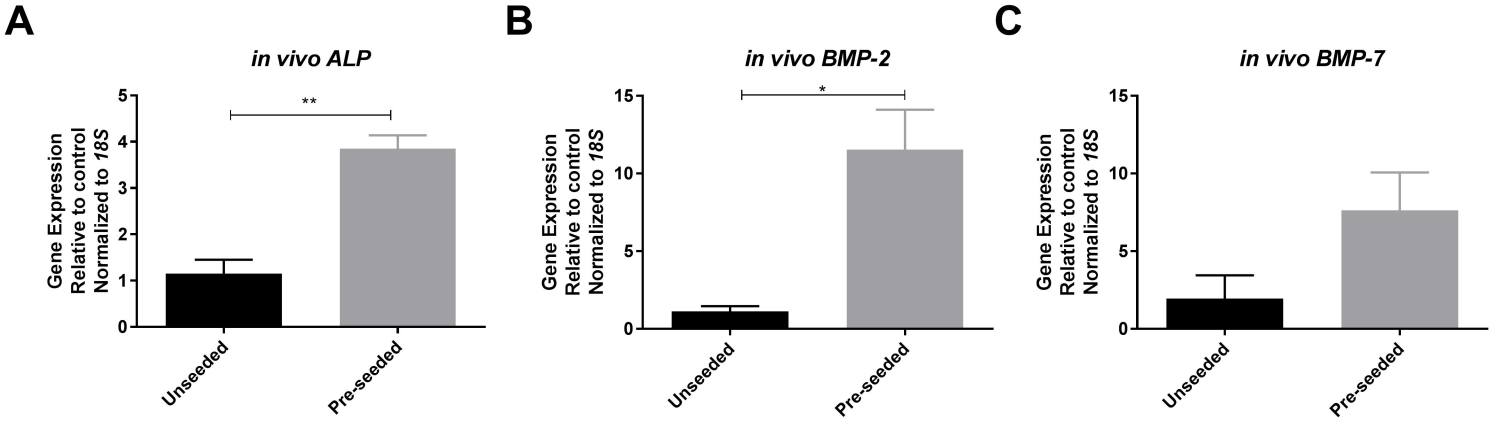
A
in vivo ALP
Gene Expression
Relative to control
Normalized to 18S
5
4
3
2
1
0
**
Unseeded
Pre-seeded
B
in vivo BMP-2
Gene Expression
Relative to control
Normalized to 18S
15
10
5
0
*
Unseeded
Pre-seeded
C
in vivo BMP-7
Gene Expression
Relative to control
Normalized to 18S
15
10
5
0
Unseeded
Pre-seeded

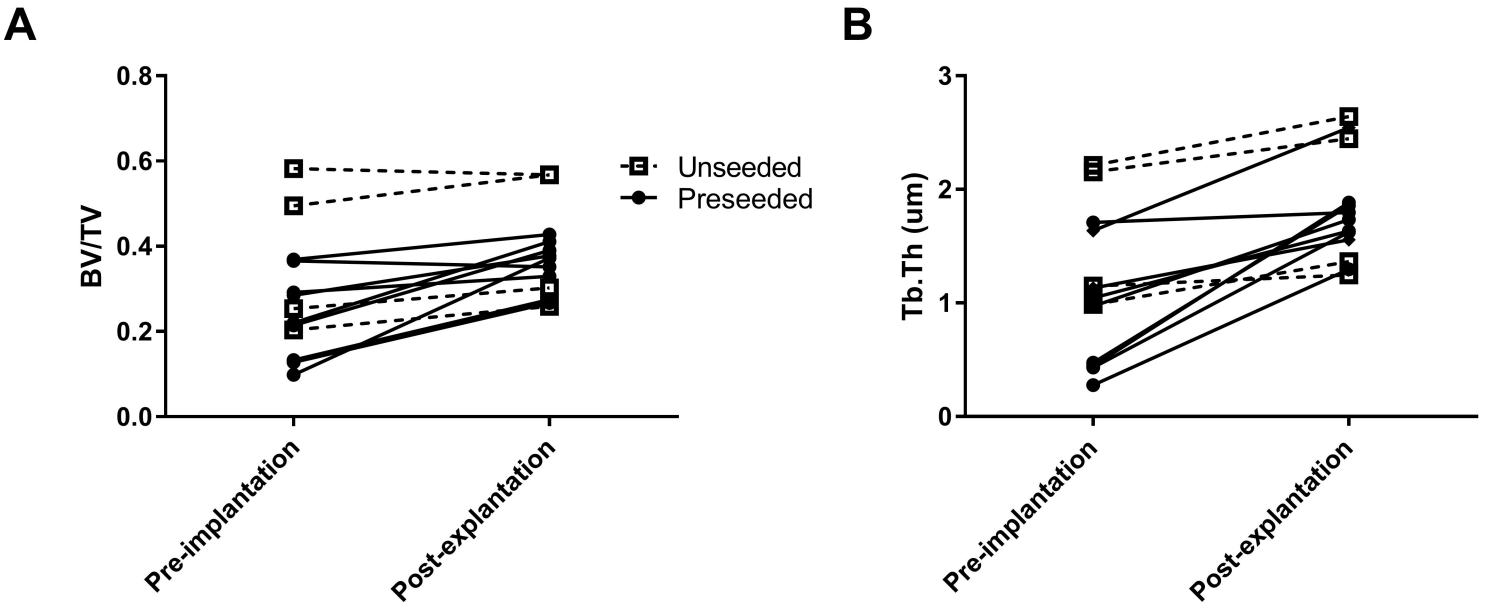
A
0.8
0.6
0.4
0.2
0.0
BV/TV
Unseeded
Preseeded
Pre-implantation
Post-explantation
B
3
2
1
0
Tb.Th (um)
Pre-implantation
Post-explantation

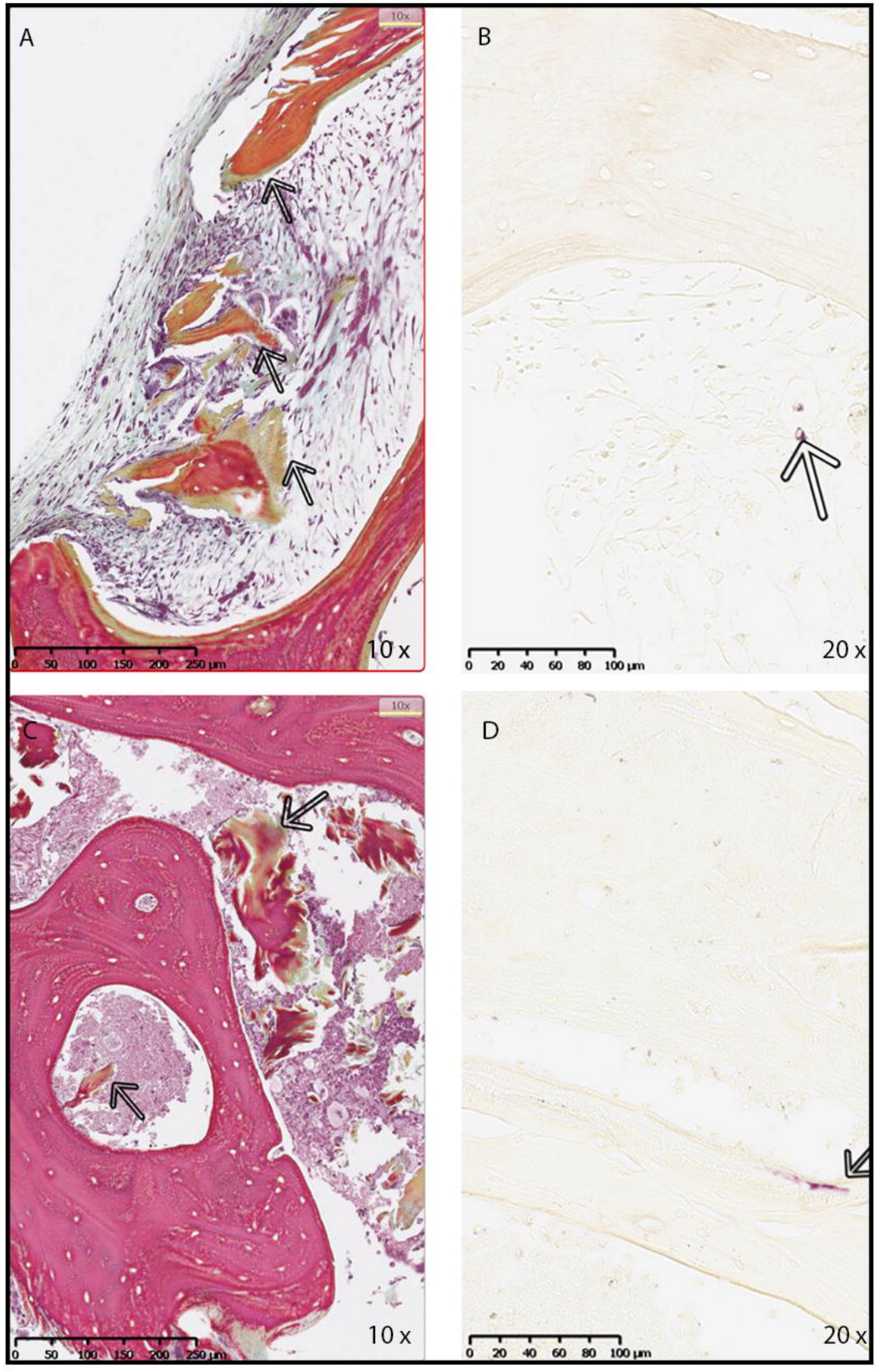
Pentachrome
TRAP
Preseeded Scaffolds
Unseeded Scaffolds
A
B
C
D
10 x
20 x
10 x
20 x

Pentachrome

CD31

Preseeded Scaffolds
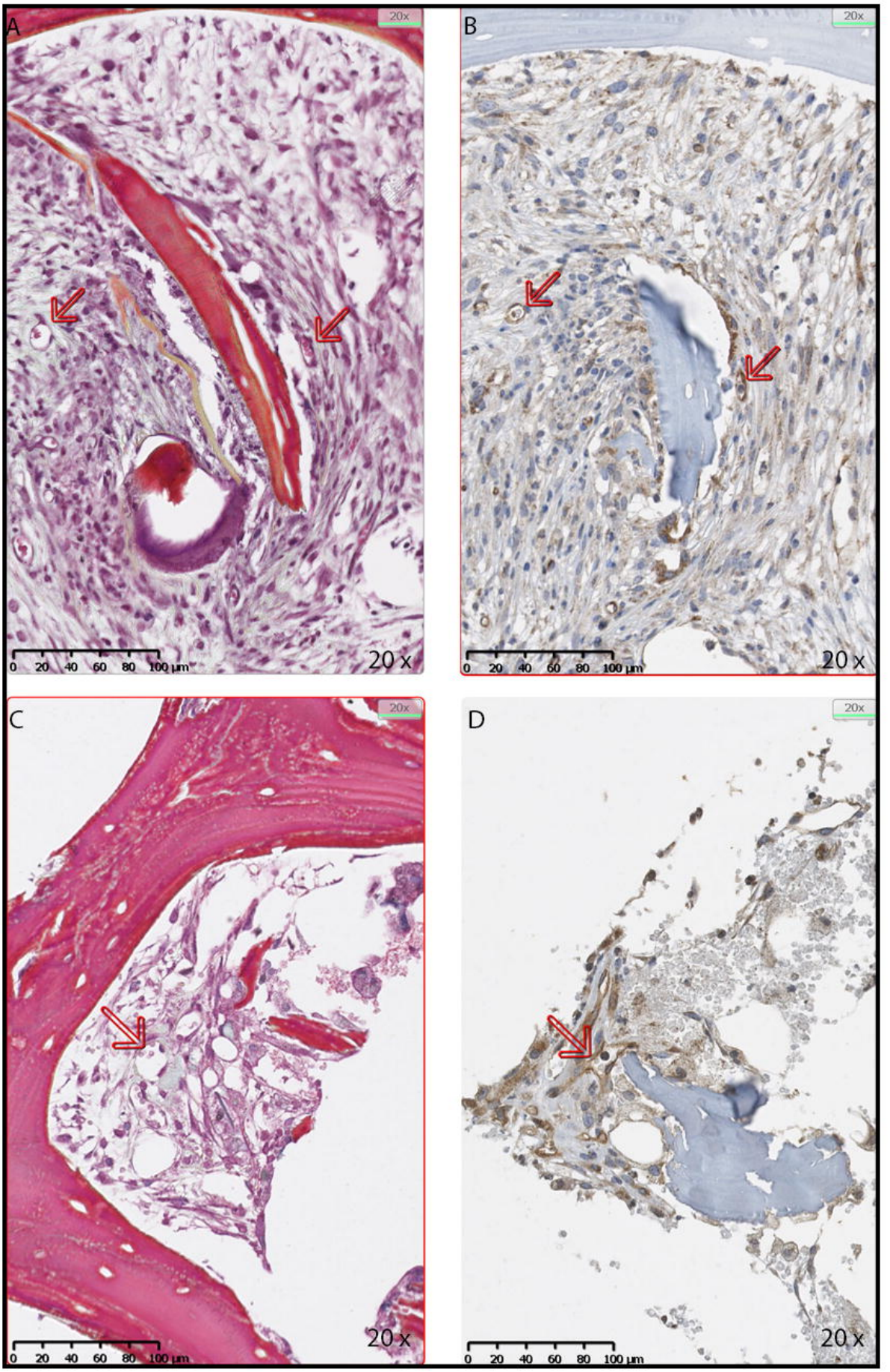
Unseeded Scaffolds